Numerical simulation of landslides after slope failure using MPM with SYS Cam-clay model in shaking table tests

K. Abe, M. Shinoda, K. Watanabe, T. Sanagawa & S. Nakajima
Railway Technical Research Institute, Japan

S. Nakamura
Nihon University, Japan

T. Kawai
Tohoku University, Japan

M. Murata & H. Nakamura
Japan Nuclear Energy Safety Organization, Japan

SUMMARY
The seismic safety of slopes is generally estimated through stability analysis focusing on the conditions prevalent before slope failure. However, it is also important to understand post-slope-failure conditions. Accordingly, a series of shaking table tests was carried out with small-scale slope models, with the results showing that the failure patterns of landslides involve progressive deformation and catastrophic failure. In order to establish a methodology for the elucidation of failure patterns, the authors carried out landslide simulations using the material point method (MPM), which allows consideration of extensive soil deformation based on the elasto-plastic constitutive law. Here, the super/subloading yield surface Cam-clay model (SYS Cam-clay model) was adopted for this purpose. The outcomes showed that a landslide mass behavioral trend similar to that seen in the shaking table tests can be obtained using the MPM with the SYS Cam-clay model.

Keywords: slope failure during earthquakes, material point method, SYS Cam-clay model

1. INTRODUCTION

The seismic safety of slopes is generally estimated through stability analysis based on a simplified conservative approach such as the Fellenius method or the finite element method (FEM) with focus on pre-failure slope conditions. However, it is also important to quantitatively understand the conditions of slopes after failure and determine the displacement of landslide masses. A series of shaking table tests carried out by Nakamura et al. (2011) with small-scale slope models revealed that the failure patterns of landslide masses varied with the test model characteristics. The failure patterns involved progressive deformation and catastrophic failure, and it was considered important to estimate these patterns before slope collapse occurs. To support the determination of such patterns, an analytical method is needed that allows consideration of extensive soil deformation with properties introduced from ground surveys such as triaxial compression tests using actual slope samples. Strain softening in drained conditions also plays a significant role in the characteristics of landslides after slope failure, particularly in lower-strength layers. Toward the establishment of such an analytical method, we carried out simulations of post-failure landslides in shaking table tests using the material point method (MPM) (Sulsky et al., 1995), which is a particle-in-cell numerical approach that allows seamless treatment of considerations from elastic behavior to discontinuous collapse behavior of soil based on the elasto-plastic constitutive law. For this purpose, we adopted the super/subloading yield surface Cam-clay model (SYS Cam-clay model) (Asaoka et al., 2000), which can deal with the degradation processes that bring about changes in soil from a structured state to a destructured state. The study showed that the results obtained from landslide mass behavior simulations according to the slope model type (e.g., progressive deformation and catastrophic failure) were the same as those seen in the shaking table tests using the MPM with the SYS Cam-clay model as the constitutive law.

2. SHAKING TABLE TESTS

2.1. Test outline and models

Figure 2.1 shows the initial states of the test models. For classification, the models are referred to here as follows:
Model 1: Three-layer model with a weak layer on a slope of 45 degrees and a height of approx. 1.0 m
Model 2: Three-layer model with a weak layer on a slope of 35 degrees and a height of approx. 1.0 m
Model 3: Three-layer model with a weak layer on a slope of 45 degrees and a height of approx. 2.0 m
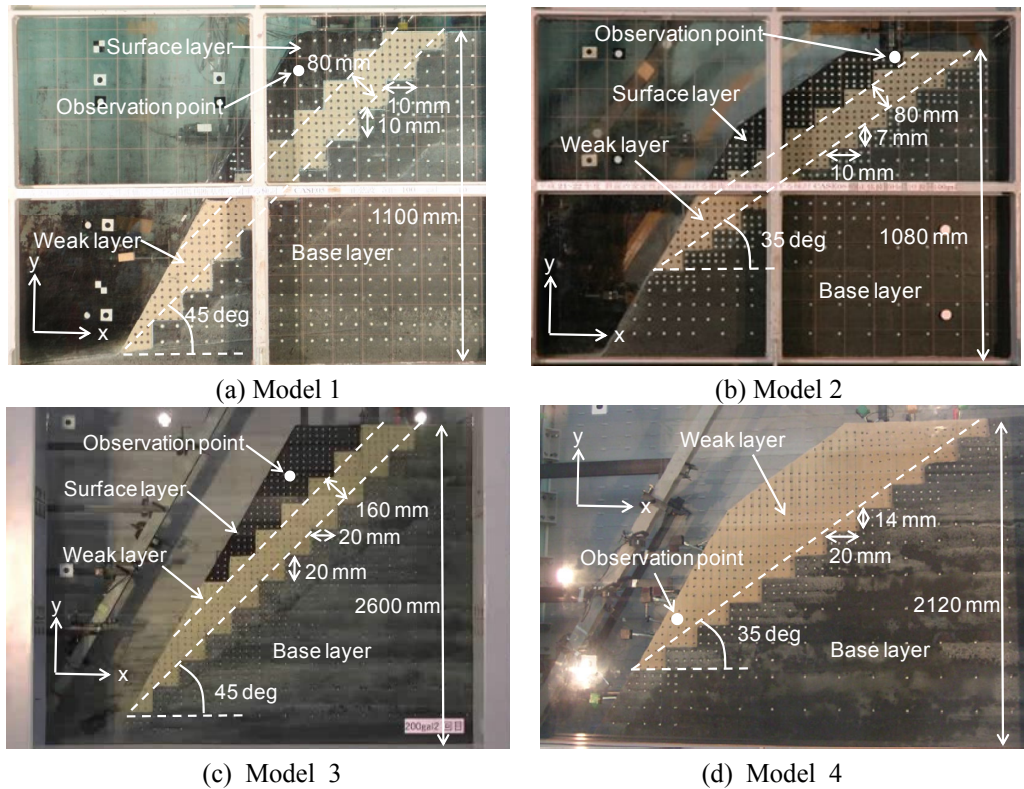Model 4: Two-layer model with a boundary on a slope of 35 degrees and a height of approx. 2.0 m

(a) Model 1   (b) Model 2

(c) Model 3   (d) Model 4

Figure 2.1. Test models (initial state)

Table 2.1. Representative parameters of the models used in the shaking table tests

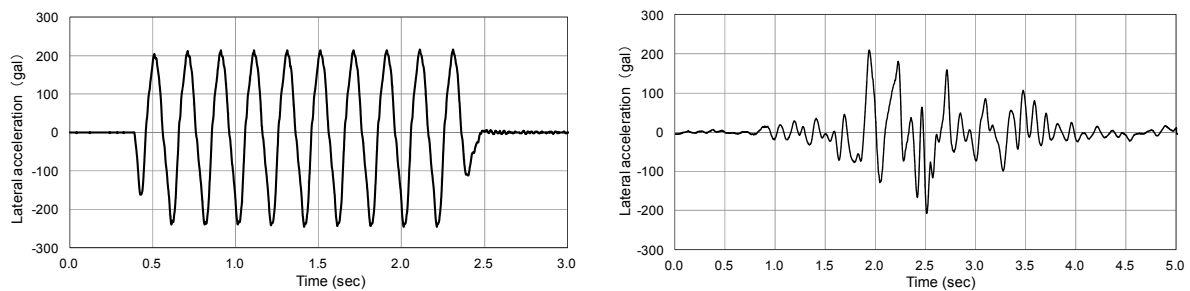| Model no.	Gradient of weak layer (deg.)	Width of weak layer (mm)	Height (mm)	Width (mm)
1	45	80.0	1,100	600
2	35	80.0	1,080	600
3	45	160.0	2,600	1,200
4	—	—	2,120	1,200

Figure 2.2. Examples of waves input in the shaking table tests (left: sine wave; right: irregular wave)

Table 2.1 shows representative parameters of the shaking table test models, which were three-layer and two-layer types. The three-layer models were based on the assumption that some rock slopes have a lower-strength cohesive sand layer that significantly influences landslide characteristics at the post-slope-failure stage. These models had a surface layer, a weak layer and a base layer. The weak layer was a lower-strength cohesive sand stratum with properties similar to those seen in actual rock slopes. The gradients of the weak layers were different in each model at 35 and 45 degrees. The three-layer models were made with heights of approximately 1.0 m and 2.0 m to allow investigation of how model size affects the characteristics of landslides after slope failure occurs. We also used two types of input waves in the shaking table tests – a 5-Hz sine wave with a wavenumber of 10 and an irregular wave (**Figure 2.2**) to clarify how the input wave type influences these characteristics. The former wave type was used in the tests with models 1 and 2, and the latter was used in that with Model 3. The shaking table for the tests with models 1 and 2 was 2.0 m long and 1.0 mm high, and that for Model 3 was 4.0 m long and 2.0 m high. **Table 2.2** shows the three-layer slope model soil properties as determined from triaxial compression testing with the materials in the layers, which were made so that the strength of the weak layer was the lowest and the self-weight of the surface layer was the highest. The base layer was made of dense crushed stone stabilized with cement and reinforced using transverse anchors fixed to the shaking table. The weak layer was made of siliceous sand mixed with bentonite (1% by weight), and the surface layer was iron powder mixed with bentonite (10% by weight) to increase its self-weight. To prevent sliding at the divisions between layers, the boundaries were bench-cut as shown in **Figure 2.1**. Openings of 4.0 mm or 8.0 mm were also left between the slope models and the acrylic or glass sidewalls of the shaking table to ensure that there were no frictional forces between the models and the walls. The response of the models was investigated using accelerometers, displacement transducers and analysis of images taken via a high-speed CCD camera with focus on the dynamic characteristics of landslides.

The two-layer model was based on the assumption that some rock slopes have a thick lower-strength cohesive sand weather layer that significantly influences landslide characteristics at the post-slope-failure stage. The two-layer model had a weak layer and a base layer. The weak layer was a lower-strength cohesive sand stratum identical to that of the three-layer models. The gradient of the boundary between the weak layer and the base layer was 35 degrees, and the boundary had a bench cut as with the three-layer types. The model was about 2.0 m in height, and a 5-Hz sine wave with a wave number of 10 was used as the input wave in the shaking table test as shown in **Figure 2.2**. The shaking table was 4.0 m long and 2.0 m high, and the response of the slope model was investigated in the same way as for the three-layer models.

The maximum amplitude of the input waves was increased with stepwise changes as shown in **Table 2.3**. The manner in which the amplitude of the input waves was changed differed among the models. However, all models exhibited tension cracking at the top of the slope when the input wave amplitudes reached 400 gal for Model 1, 600 gal for Model 2, 200 gal for Model 3 and 450 gal for Model 4, and slope failure subsequently occurred. Signs of tension cracking were seen at the top of the slope just before the final step in models 1, 2 and 3, and no clear signs were observed in Model 4.

Table 2.2. Soil properties of the test model layers

Layer	Density (kg/m³)	Peak state		Residual state	
		Cohesion (kPa)	Internal friction angle (deg.)	Cohesion (kPa)	Internal friction angle (deg.)
Surface layer	3,000	107	0.0	34.4	28.4
Weak layer	1,767	2.9	39.5	1.7	36.3
Base layer	1,890	280.5	57.3	5.4	53.4

Table 2.3. Maximum amplitudes of waves input in stepwise changes

Model no.	Order of input wave maximum amplitudes
1	100 gal → 200 gal → 300 gal → 400 gal[*]
2	100 gal → 200 gal → 300 gal → 400 gal → 500 gal → 600 gal[*]
3	50 gal → 100 gal → 200 gal → 200 gal[*]
4	100 gal → 200 gal → 300 gal → 350 gal → 400 gal → 450 gal → 500 gal → 200 gal → 300 gal → 350 gal → 400 gal → 450 gal[*]

*Maximum amplitude of input wave under which slope failure occurred

2.2. Test results

Figure 2.3 shows the final configurations of the post-failure test models. The failure type of each was different: Slide-down was seen along the slip surface in the weak layer when the amplitude of the input wave was 400 gal in Model 1 and 200 gal in Model 3 (i.e., the models with a steep gradient of 45 degrees for the weak layer), while progressive deformation was seen along the slip surface in the weak layer when the input wave amplitude was 600 gal in Model 2 (i.e., the model with a gentle gradient of 35 degrees for the weak layer). The two-layer Model 4 exhibited catastrophic failure starting from collapse at the toe of the slope when the input wave amplitude was 450 gal; that is, the toe of the model's weak layer failed in the initial failure stage, and the model then exhibited progressive deformation and discontinuous collapse around the toe of the slope.
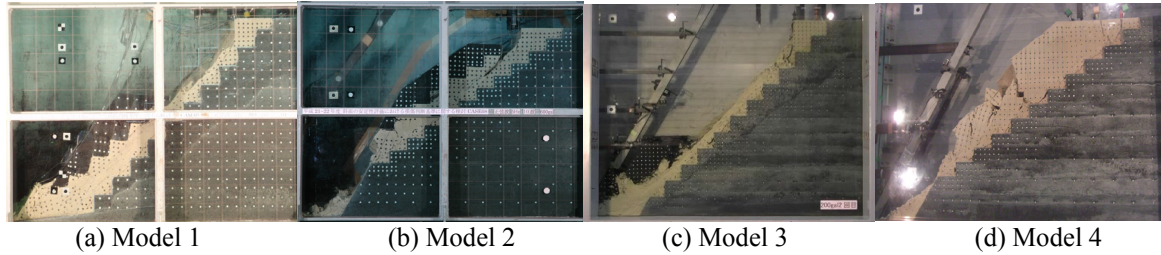

(a) Model 1   (b) Model 2   (c) Model 3   (d) Model 4

Figure 2.3. Final configurations of the post-failure test models
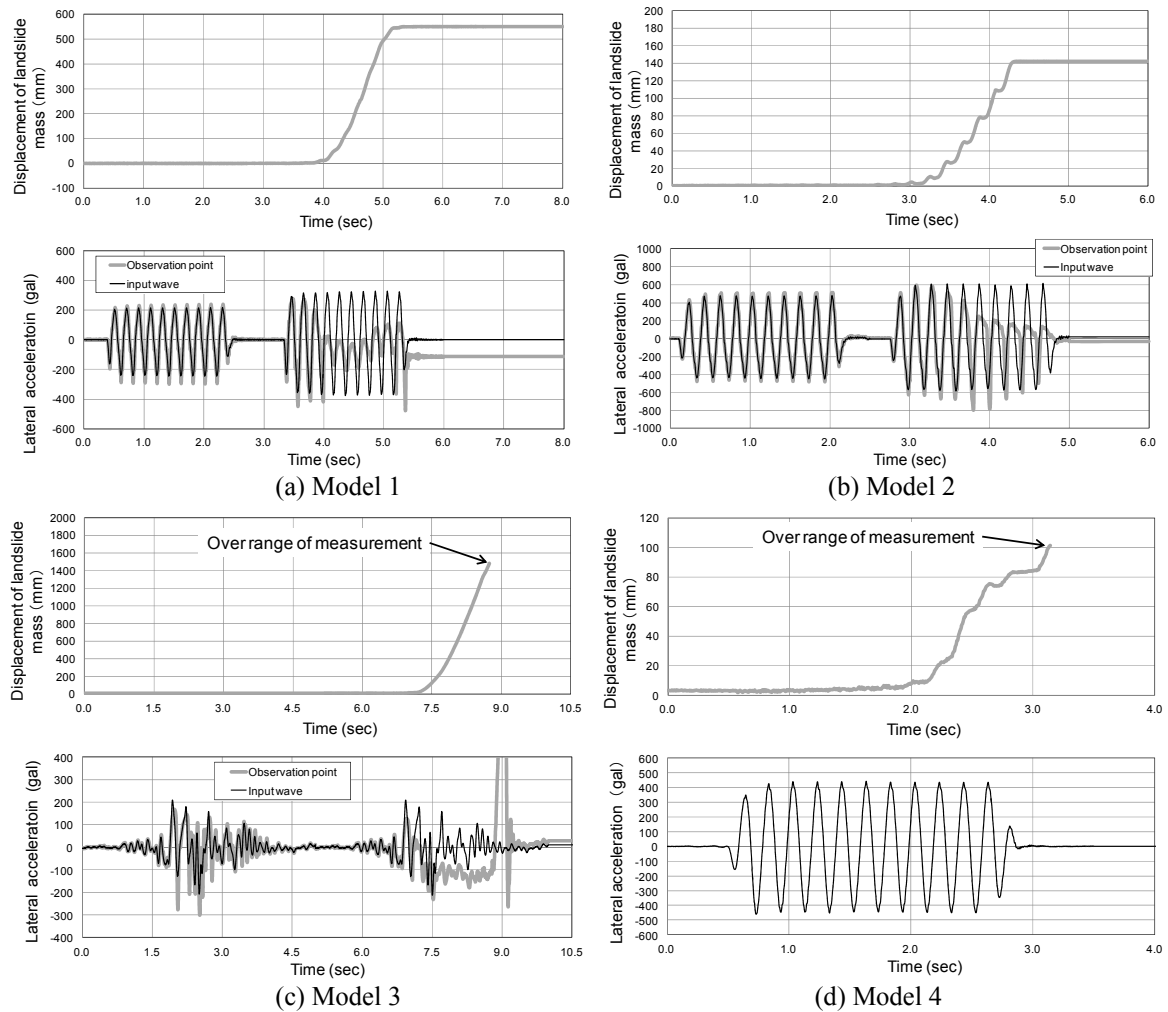

Figure 2.4. Time histories of displacement and acceleration at observation points

Figure 2.4 shows time histories of displacement at the observation points defined in **Figure 2.1** at the final step as slope failure occurred and in the penultimate step when signs of tension cracking were seen at the top of models 1, 2 and 3. Data collected between the penultimate and final steps were discarded because the slope models did not exhibit any particular behavior at this time. The behavior of Model 4 at the penultimate step was also not investigated because the model did not show particular signs of slope failure in contrast to the others. The time histories shown here were extracted from analysis based on images captured by the high-speed CCD camera. For models 1, 2 and 3, the displacement time histories are for the surface layer mass, while that for Model 4 is for the portion where collapse at the toe of the weak layer occurred. It can be seen that these histories reflect the failure patterns described previously.

Figure 2.4 shows time histories of acceleration at the observation points on the slope models (except for Model 4) as defined in **Figure 2.1** at the final stage as slope failure occurred and at the penultimate stage. The positions of the observation points are same as those for the displacement time histories. It can be seen from the results for models 1 and 2 that the acceleration of the surface layer mass was almost constant in movement under progressive deformation, and that it then approached zero when rapid slide-down occurred. This indicates that the yield acceleration of the mass became zero when slide-down was seen in the slip surface of the weak layer, and implies that rapid slide-down occurred when the horizontal-yield seismic coefficient became zero.

3. SIMULATIONS USING THE MPM WITH THE SYS CAM-CLAY MODEL

3.1. Outline of the MPM with the SYS Cam-clay model

3.1.1. Outline of the MPM
With the conventional FEM, it can be difficult to solve large deformation problems because excessive remeshing of mesh distortions is required. A number of mesh-free methods have been proposed to overcome this, including the use of smoothed particle hydrodynamics (SPH) (Lucy, 1977; Gingold and Monaghan, 1977) and the MPM (Sulsky et al., 1995). Recently, the MPM has gained popularity for solving problems with a large deformed continuum. The approach utilizes Lagrangian particles that carry all physical parameters such as stress, density and history variables. The particles move freely across boundaries of a stationary Eulerian computational background mesh that covers their positions as shown in **Figure 3.1**. The method is computationally efficient because the background mesh is used to solve the equation of motion in a manner similar to that of the conventional FEM (see **Figure 3.1**). The use of a background mesh also facilitates the implementation of boundary conditions as compared to other mesh-free methods. The technique has also recently been applied to soil for cases of particular slope failure because considerations ranging from elastic behavior to discontinuous collapse behavior of soil can be seamlessly considered based on the elasto-plastic constitutive law.

The general MPM developed by Sulsky et al. (1995) involves explicit time-marching calculation. The domain of the body analyzed in a two-dimensional plane strain condition is composed of the sub-domains Ω_p, $p = 1, ..., N_p$. Each sub-domain is associated with a reference particle, as defined by the position vector $\mathbf{x}_p^k = \left(x_p^k, \ y_p^k \right)$, the mass m_p and the volume V_p. Superscript k denotes the evaluation at time t^k. The analytical flow of the adapted MPM used in this study was almost the same as that of the general MPM developed by Sulsky et al. However, wave attenuation was included in the equations of motion, which were solved at the nodes of the background meshes using the following equation in consideration of Rayleigh damping:

$$\mathbf{f}_i^{dmp} = -\alpha \sum_p^{N_p} m_p N_i\left(\mathbf{x}_p\right)\mathbf{v}_p - \beta \sum_p^{N_p} \frac{m_p}{\rho_p} \left\{ \nabla N_i\left(\mathbf{x}_p\right) \cdot \left(\mathbf{T}_p^E : \frac{\Delta \boldsymbol{\varepsilon}_p}{\Delta t} \right) \right\} \tag{3.1}$$

where $\mathbf{f}_i^{dmp}$ is the damping force at node i of the stationary Eulerian computational mesh, $N_i(\mathbf{x}_p)$ is an interpolation function of node i at $\mathbf{x}_p$, $\mathbf{v}_p$ is the velocity of particle p, ρ_p is the density of particle p, $\Delta\varepsilon_p$ is the strain increment of particle p, $\mathbf{T}_p^E$ is the elastic stiffness of particle p, Δt is the time interval, and

α and β are damping constants. The first term on the right-hand side of the equation describes mass proportional damping and the second describes stiffness proportional damping. For the damping constants α and β, values of 0.0 and 0.002 were set, respectively.
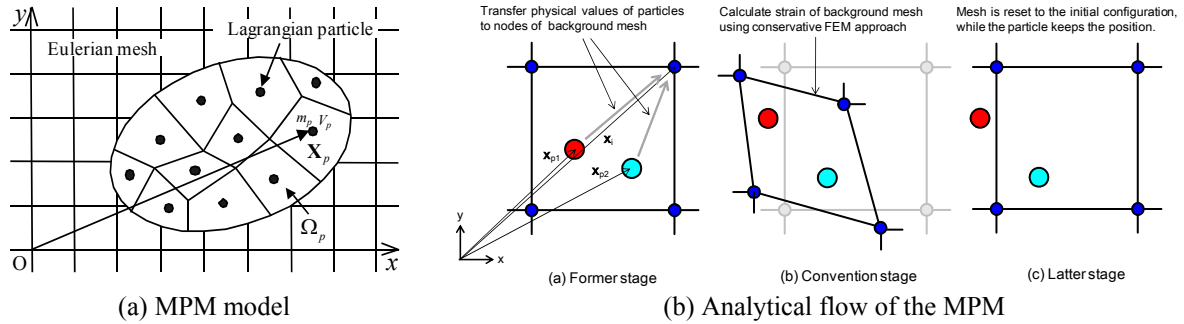

(a) MPM model

(b) Analytical flow of the MPM

Figure 3.1. Schematic figures of the model and the analytical flow of the MPM

3.1.2. Outline of the SYS Cam-clay model

The SYS Cam-clay model was developed by Asaoka et al. (2000), and can describe the degradation processes from both an overconsolidated state to a normally consolidated state and from a structured state to a destructured state – processes that play an important role in the plastic deformation of soil. These are described based on the superloading yield surface concept together with Hashiguchi's subloading yield surface concept. In the SYS Cam-clay model, the corrected Cam-clay model of Roscoe and Burland (1968) with the rotational hardening concept of Sekiguchi and Ohta (1977) added is used as a normal yield surface to describe soil in an unstructured and normally consolidated state, which may still be anisotropic. In particular, it is considered that the degradation processes leading from a structured state to a destructured state described by the superloading yield surface will affect the dynamic characteristics of post-slope-failure landslides because the technique allows the representation of strain softening in soil under drained conditions, which plays an important role in the generation of surface slippage on slopes and in the dynamic characteristics of landslides. Specifically, the generation of surface slippage on a slope depends on progressive failure along the surface, and the dynamic behavior of landslides depends on the residual strength of the slip surface.

Figure 3.2 shows the results of investigation to determine the stress-strain characteristics of a material specimen in a weak layer under triaxial compression testing and cyclic triaxial testing using the SYS
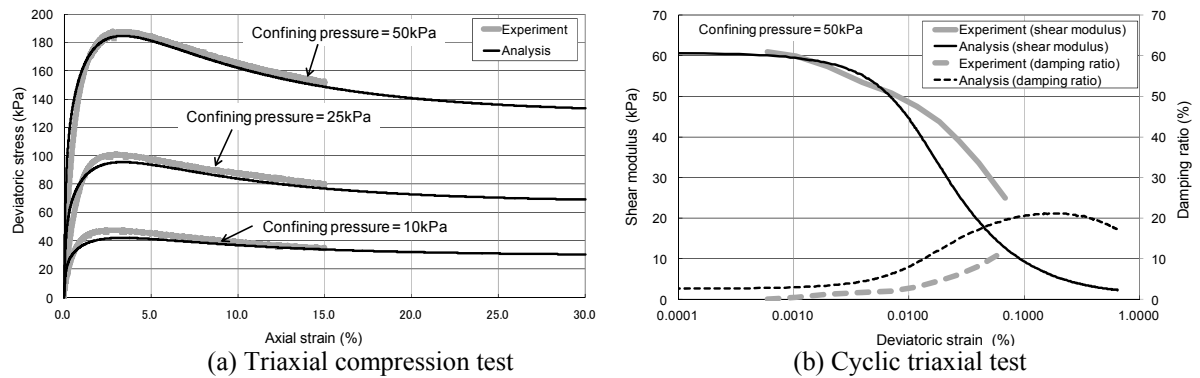

(a) Triaxial compression test

(b) Cyclic triaxial test

Figure 3.2. Results of investigation to determine the stress-strain characteristics of weak-layer material

Table 3.1. Parameters of the SYS Cam-clay model

Compression index	0.01 – 0.15	Degradation parameter of structure	0.01
Swelling index	0.001 – 0.14	Degradation parameter of overconsolidated state	0.001
Critical state constant	1.37	Evolution index of rotational hardening	5.0
Poisson's ratio	0.214	Limit of rotational hardening	1.35
Degree of anisotropy	0.75	Specific volume at $q = 0$ and $p\,'= 98.1$ kPa on NCL N	2.085
Degree of structure	3.3	Overconsolidation ratio	3.3

Cam-clay model with the parameters shown in **Table 3.1**. This indicates that the model can be used to describe the stress-strain characteristics of a material in a weak layer with a high level of accuracy. To produce the most accurate cyclic triaxial test results possible, we increased the compression index λ and the swelling index κ in accordance with cumulative shearing strain as proposed by Uzuoka (2000).

3.2. Simulation models and results

3.2.1. Simulation models and parameters
Figure 3.3 shows schematic representations of the simulation models in their initial states. The SYS Cam-clay model was used for the weak layer of the models, while the perfect elasto-plastic Drucker-Prager model (Drucker and Prager, 1952) and the elasticity model with the constitutive law were used for the surface and base layers, respectively. The parameters were determined based on the results of triaxial compression testing on samples from these layers as shown in **Table 2.2**.
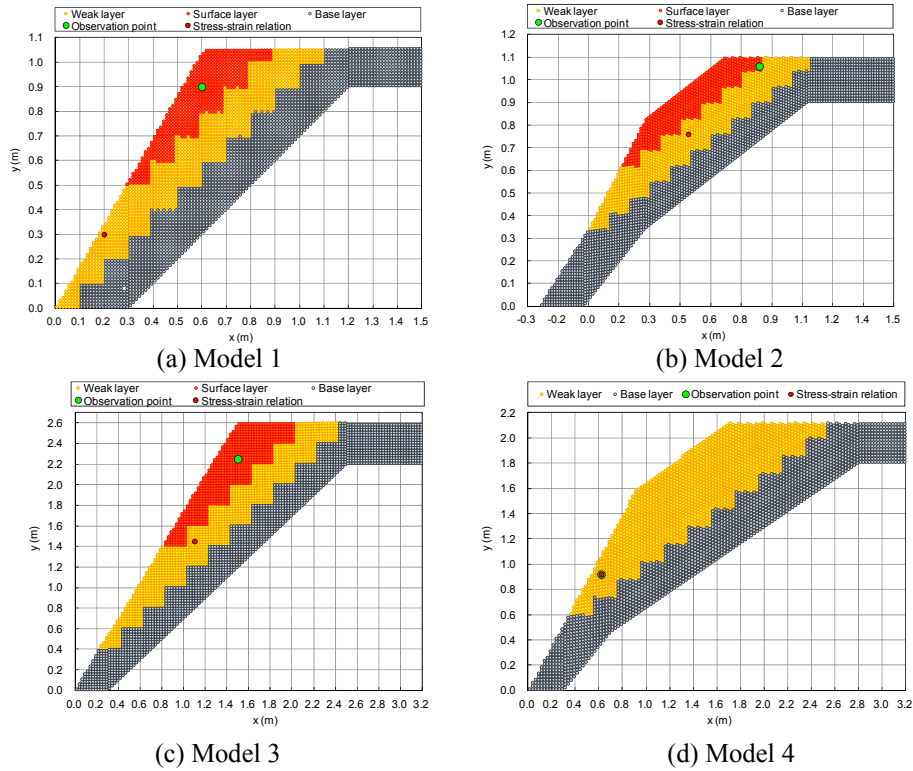

(a) Model 1   (b) Model 2

(c) Model 3   (d) Model 4

Figure 3.3. Schematic representations of the simulation models in their initial states

3.2.2. Simulation results
Figure 3.4 shows the processes of slope model deterioration in the simulation along with the final configurations of the models in the experiments. The contours in the figures represent the magnitude of the maximum shear strain in the slopes. The final configurations are largely consistent with those of the experiment, with large maximum shear strain in the weak layer of the slope models. This indicates that the simulation is appropriate for describing the final slope configuration, although conservative FEM cannot deal with large instances of deformation such as discontinuous collapse. The figures also indicate that the simulation results describe the trend of the outcomes from the shaking table tests on the slope models, i.e., slide-down along the slip surface in the weak layer as seen in Model 1 and Model 3, progressive deformation of the surface layer as seen in Model 2, and discontinuous collapse behavior at the toe of the slope as seen in Model 4. Specifically, the simulation results for Model 1 and Model 3 show rapid development of surface slippage in the weak layer and then rapid slide-down along this surface, while those for Model 2 show progressive deformation of the surface layer together with development of surface slippage in the weak layer. Model 4 also shows the development of shear strain at the toe of the model and the subsequent occurrence of discontinuous collapse around the toe.

However, the simulation models do not describe the final configurations due to traces of tension cracking at the top of the weak layer in models 1, 2 and 3. The scale of plastic deformation at the top and discontinuous collapse at the toe of Model 4 is larger than those seen in the experiments. This is thought to be due to a lack of consideration for cohesive strength in zones of low confining pressure and tension. Model 4 was also affected by the 500-gal input wave before the final step. This influence should be investigated in future work.
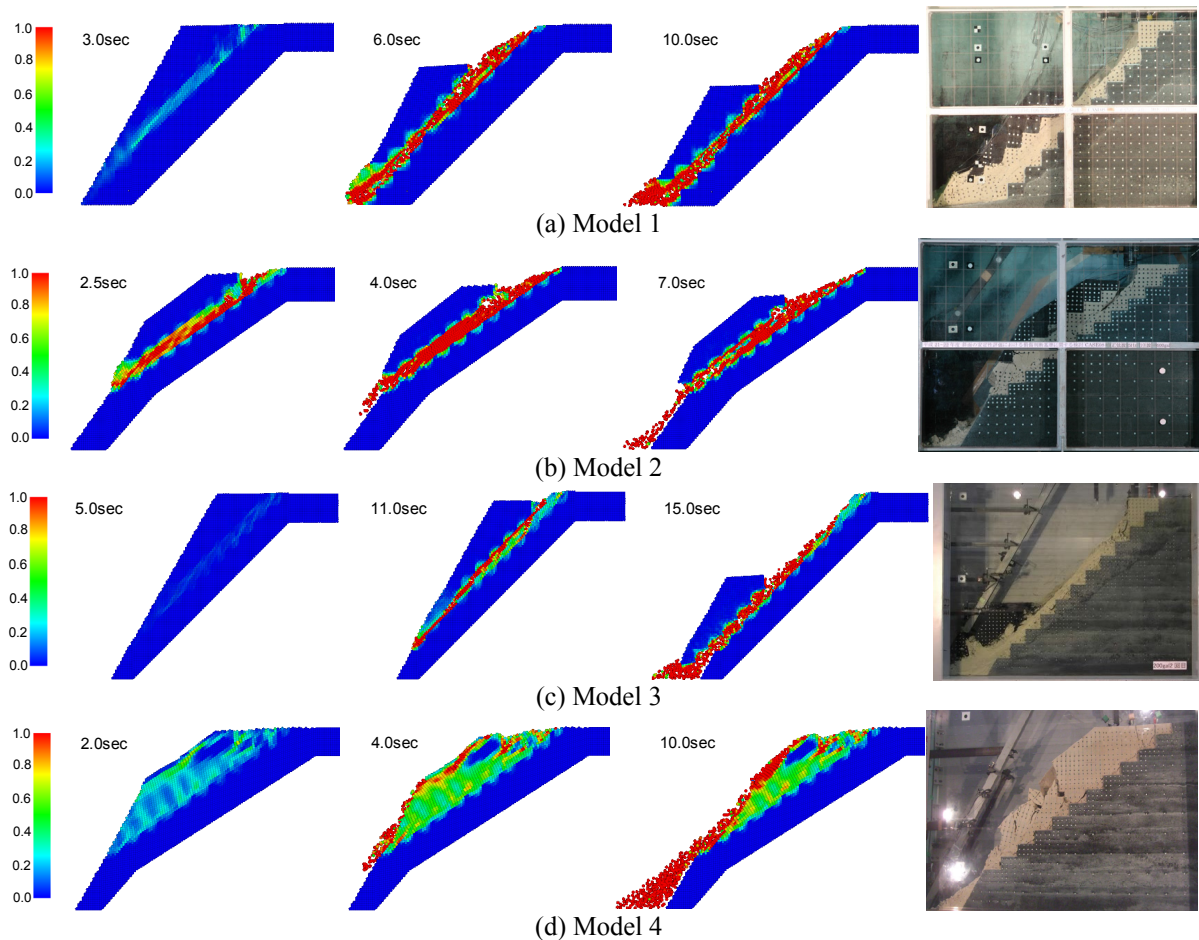

(a) Model 1

(b) Model 2

(c) Model 3

(d) Model 4

Figure 3.4. Slope model deformation processes in the simulation (contours: maximum shear strain)

Figure 3.5 shows the results of simulation for the time histories of displacement at the observation points on the slope models displayed in **Figure 3.3**. The histories for all models except Model 4 are for the surface layer, and that of Model 4 is for the toe of the slope where catastrophic failure occurred. The outcomes of image analysis in the shaking table tests are also given for these observation points, and comparison with the simulation results was conducted. For Model 1, the start time of displacement in the simulation is largely consistent with that in the experiment, but the rate of change for displacement in the simulation is different. For Model 2, the start time of displacement is different, but the rate of change in displacement is largely consistent with that in the experiment. For Model 4, both the start time and the rate of change of displacement in the simulation are largely consistent with those in the experiment within the range captured via image analysis. For Model 3, the start time of displacement in the simulation is different from that in the experiment. This is considered to stem from the simulation's lack of consideration for treatment of the influences of irregular input waves on the dynamic characteristics of landslides.

Figure 3.5 shows the results of simulation for the time histories of lateral acceleration at the observation points of the slope models (except Model 4) displayed in **Figure 3.3**. The measurements from accelerometers installed near the observation points in the shaking table tests are also given, and comparison with the simulation results was conducted. In the experiments, acceleration in the mass of

the surface layer was found to be almost constant with movement under progressive deformation, but approached zero when rapid slide-down occurred. The simulation results show the trend observed in the experiment on Model 1, but it is less clear than that seen in the experimental results as for other models. This is considered to stem from the numerical noise of the MPM in regard to acceleration and a lack of description for post-slope-failure landslide characteristics, which influenced the accuracy of the simulation results.
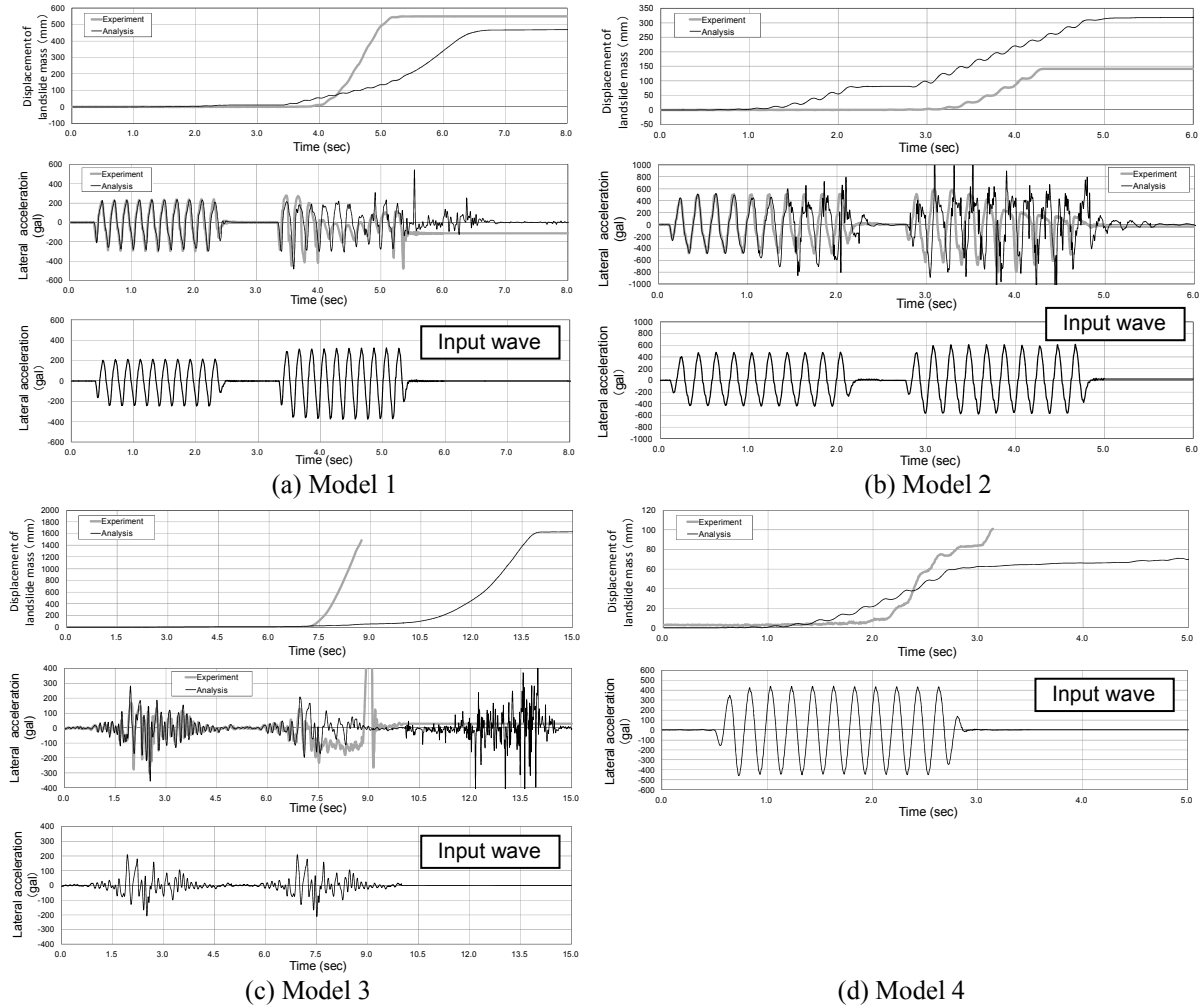

(a) Model 1

(b) Model 2

(c) Model 3

(d) Model 4

Figure 3.5. Time histories of landslide mass displacement and lateral acceleration at the observation points of the slope models in the simulation

Figure 3.6 shows the results of simulation for the relationships between the square root of the second invariant of deviatoric stress tensor and strain tensor values of less than 1.2 at the stress-strain relation points shown in **Figure 3.3**. These relationships depend on the magnitude of strain/confining stress and the change in slope geometry. Strain softening can be seen at parts where progressive failure and discontinuous collapse occurred. This is considered to imply that the characteristics of strain softening under drained conditions (i.e., the processes of degradation from a structured state to a destructured state) play an important role in the characteristics of post-slope-failure landslides.

4. CONCLUSIONS

This paper describes the results of shaking table tests and simulation using the MPM with the SYS Cam-clay model for slope failure during seismic activity. The outcomes can be summarized as
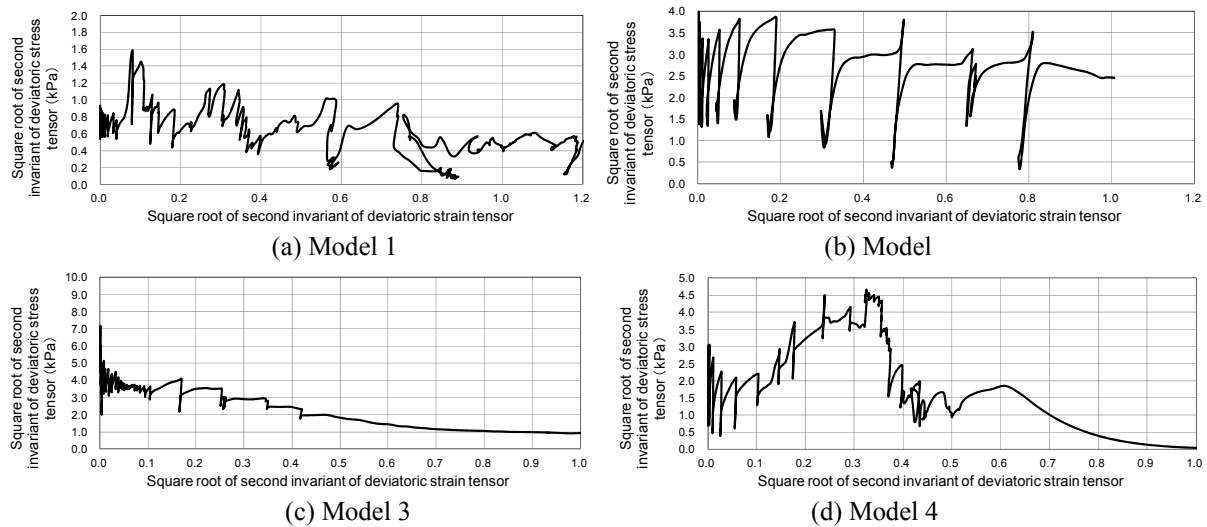
(a) Model 1

(b) Model

(c) Model 3

(d) Model 4

Figure 3.6. Stress-strain relationships at the stress-strain relation points of the slope models

follows:

1) The failure patterns of landslide masses depended on the gradient of the slip surface in the weak layer, and failure tended to start from collapse at the toe of the slope in the slope model without a surface layer.

2) A time history representation indicated that acceleration of the surface layer mass is almost constant when it moves under progressive deformation, but is nearly zero when the mass slides down rapidly. This implies that when slide-down occurs, the horizontal yield seismic coefficient becomes zero.

3) The simulation results appropriately described the trend of the outcomes from the shaking table tests on progressive deformation as well as slide-down and discontinuous collapse behavior. This indicates that the use of the MPM can support estimation of the characteristics and displacement of large deformed slopes regardless of the slope failure type.

4) Simulation did not produce accurate results regarding the start time of displacement and the lateral acceleration of the landslide mass in some models. These needs to be improved in future work.

5) The simulation results for the relationships between the square root of the second invariant of deviatoric stress tensor and strain tensor implied strain softening, which can be described by the SYS-Cam clay model, plays an important role in the characteristics of post-slope-failure landslides.

REFERENCES

Asaoka, A., Nakano, M. and Noda, T. (2000). Superloading yield surface concept for highly structured soil behavior. *Soils and Foundations* **40: 2**, 99 – 110.

Drucker, D. C. and Prager, W. (1952). Soil mechanics and plastic analysis for limit design. *Quarterly of Applied Mathematics* **10: 2**, 157 – 165.

Gingold R. A. and Monaghan J. J. (1977). Smoothed particle hydrodynamics: theory and application to non-spherical stars. *Monthly Notices of the Royal Astronomical Society* **181**, 375 – 389.

Lucy, L. (1977). A numerical approach to testing the fission hypothesis. *Astronomical Journal* **81**, 1013 – 1024.

Nakamura, H., Murata, M., Shinoda, M., Watanabe, K., Sanagawa, T., Kawai, T. and Nakamura, S. (2011). Study on the characteristics of damage on rock slope models in accordance with different weak layers in a shaking table test. *Proc. 66th JSCE Annual Meeting, Matsuyama*. 573 – 574 (in Japanese).

Roscoe K. H. and Burland J. B. (1968). On the generalised stress-strain behaviour of 'wet' clay, Eng. plasticity, Cambridge Univ. Press, 535 – 609.

Sekiguchi, H. and Ohta, H. (1977). Induced anisotropy and time dependency in clays. *Proc. 9th ICSMFE Specialty Session 9, Tokyo*. 229 – 237.

Sulsky, D., Zhou, S. J. and Schreyer, H. L. (1995). Application of a particle-in-cell method to solid mechanics. *Computer Physics Communications* **87**, 236 – 252.

Uzuoka R. (2000). Analytical study on the mechanical behavior and prediction of soil liquefaction, PhD thesis, Gifu University, 49 – 76 (in Japanese).